

Article

Iron Oxide/Salicylic Acid Nanoparticles as Potential Therapy for B16F10 Melanoma Transplanted on the Chick Chorioallantoic Membrane

Maria Cristina Predoi ^{1,†}, Ion Mîndrilă ^{1,*}, Sandra Alice Buteică ^{2,†}, Ștefana Oana Purcaru ^{3,†}, Dan Eduard Mihaiescu ⁴ and Ovidiu Marcel Mărginean ¹

¹ Department of Morphology, Faculty of Medicine, University of Medicine and Pharmacy of Craiova, 200349 Craiova, Romania; predoi.cristina@yahoo.com (M.C.P.); ommarginean@gmail.com (O.M.M.)

² Faculty of Pharmacy, University of Medicine and Pharmacy of Craiova, 200349 Craiova, Romania; alice.buteica@umfcv.ro

³ Department of Biochemistry, Faculty of Medicine, University of Medicine and Pharmacy of Craiova, 200349 Craiova, Romania; stoapo@yahoo.com

⁴ Faculty of Applied Chemistry and Materials Science, University Politehnica of Bucharest, 011061 Bucharest, Romania; danedmih@gmail.com

* Correspondence: ion.mindrila@umfcv.ro

† These authors contributed equally.

Received: 9 May 2020; Accepted: 15 June 2020; Published: 19 June 2020



Abstract: Unfavorable prognoses and low survival rates are specific features of metastatic melanoma that justify the concern for the development of new therapeutic strategies. Lately, nanotechnology has become an attractive field of study due to recent advances in nanomedicine. Using a chick chorioallantoic membrane (CAM) implanted with xenografts harvested from C57BL/6 mice with B16F10 melanoma cells, we studied the effects of iron oxide nanoparticles functionalized with salicylic acid (SaMNPs) as a form of therapy on the local development of xenotransplants and CAM vessels. The SaMNPs induced an anti-angiogenic effect on the CAM vessels, which accumulated preferentially in the melanoma cells and induced apoptosis and extensive xenograft necrosis. As a result, this slowed the increase in the xenograft volume and reduced the melanoma cells' ability to metastasize locally and distally. Further, we demonstrate the use of the chick CAM model as a tool for testing the action of newly synthesized nanocomposites on melanoma xenotransplants. The SaMNPs had a therapeutic effect on B16F10 melanoma due to the synergistic action of the two components of its structure: the coating of the salicylic acid with antiangiogenic and chemotherapeutic action and the core of iron oxides with cytotoxic action.

Keywords: CAM assay; B16F10 melanoma; xenotransplant; salicylic acid; iron oxide nanoparticles

1. Introduction

Melanoma is the deadliest and most aggressive form of skin cancer with poor prognosis, low survival rates, susceptibility to relapse, and multidrug resistance tendency [1,2]. Nonmetastatic melanomas benefit from basic therapeutic options such as surgery, radiotherapy, and chemotherapy. However, combined therapeutic approaches are implemented in metastatic melanomas, including immunotherapy, photodynamic therapy, targeted therapy, or hormonal therapies [3,4]. The low survival rate of these cases requires the development of new therapeutic strategies, such as nanotherapy, which is becoming more attractive due to recent advances in nanomedicine [5–7]. Promising results have been obtained in experimental melanoma therapies that use nanoparticle systems for targeting melanoma cells as drug and gene carriers and protectors in photothermal and photodynamic therapy [8,9].

Several studies have highlighted both the links between cell elasticity and the invasive phenotype of cancer cells [10], and the role melanin has in establishing cell elasticity and the metastatic phenotype of melanoma cells [11–13]. Due to its abilities [8], nanotechnology can be a vital factor in the process of modulating the nanomechanical phenotype of melanoma cells.

Functionalized iron oxide nanoparticles offer a low cost and easy-to-process work platform, as its magnetic and toxicity properties allow their use in a wide range of biomedical applications [8,14]. Magnetic iron oxide nanoparticles have been used in cancer diagnostics and therapies as magnetically targeted drug transporters, contrast agents in MRIs [8], theragnostic agents [15], and magnetic hyperthermia agents [16].

The purpose of this work was to study the effects of SaMNP therapy on the murine melanoma nontransplant growths and on the local development of the vessels. First, we used CAMs implanted with tumor xenografts harvested from C57BL/6 mice with B16F10 melanoma. We chose to use salicylic acid as a surface coating for iron oxide nanoparticles owing to the numerous laboratory studies and clinical observations from recent years that have pointed to the anticancer activity of salicylates and the multitude of mechanisms through which salicylates exert their effects in chemoprevention, including the induction of apoptosis [17], the inhibition of angiogenesis [18], the inhibition of cyclooxygenase activity [19,20], the suppression of cyclooxygenase-2 gene transcription [21], the inhibition of NF- κ B activation [22], alterations in mitochondrial function [23,24], the inhibition of 6-phosphofructo-1-kinase activity [25], the perturbation of epidermal growth factor pathway [26], etc.

The CAM model represents a powerful and widely used tool for studying tumor growth and the metastasis of cancer cells, angiogenesis, or drug delivery systems [27–31]. Due to its natural immunodeficiency during the first two weeks of its development and the accessibility offered to its rich vascularization, CAM proved to be a versatile platform for both tumor xenografts, including in cases of melanoma [32,33], and for studying pharmaceutical and biomedical applications for newly synthesized nanocompounds [34–36].

2. Materials and Methods

2.1. Functionalized Nanoparticles Dispersion

The functionalized Fe₃O₄/salicylic acid magnetic nanoparticles were synthesized and characterized by methods previously reported by some of us [37]. The nanoparticles used in this study all had the following: (a) a hydrodynamic diameter of around 50 nm, (b) a core diameter in the 10–12 nm range, (c) a zeta potential of +39.3 mV, and (d) an iron concentration of 0.356 mg/mL.

2.2. Cell Preparation

The B16F10 melanoma cells (obtained from The Institute of Biology of the Romanian Academy) that were involved in this study were grown at 37 °C and were humidified in an atmosphere with 5% CO₂ in specific cell culture plates containing DMEM (Dulbecco's Modified Eagle's Medium, Sigma-Aldrich®) that was supplemented with a 10% fetal bovine serum, 100 U/mL penicillin, and 100 mg/mL streptomycin. The melanoma cells were harvested from the culture by trypsinization and were suspended before subcutaneous injection in a cold saline with a concentration adjusted to 1×10^6 cells/mL.

2.3. Animals

The experimental protocol followed the rules of the Committee of Ethics and Scientific Deontology of the University of Medicine and Pharmacy of Craiova (identification code: 139; date of approval: 20 December 2019). Eight-week-old female mice (n = 3) (C57BL/6) that were obtained from the University of Medicine and Pharmacy of Craiova Animal Facility were used as melanoma xenograft donors. They were kept in individual cages on a 12/12 h light/dark cycle at 21 °C and had free access to water and standard laboratory chow. The mice were shaved at the right lateral flank and were

injected subcutaneously with 0.2 mL of the B16F10 cell suspension (2×10^5 cells) under Sevorane[®] anesthesia. The local tumor growth at the injection site was assessed twice a week for four weeks by using a caliper to measure the diameter of the tumor. After four weeks, the malignant melanoma tissues from Sevorane[®]-anesthetized mice were harvested by suction with an 18 G needle assembled onto a 2 mL syringe and were used as xenografts to be implanted on CAM models. The anesthetized mice were sacrificed and autopsied for local tumor growth and distal metastasis assessment.

2.4. CAM Model

Fertilized White Leghorn eggs ($n = 25$) were incubated (at 37.5 °C and 70% relative humidity) and windowed on day three. A batch of 10 eggs was used to evaluate the effects of SaMNPs on the CAM's vessel development. On day 7, each CAM was implanted with 2 blank discs (Bioanalyse[®]): one impregnated with saline and the other with an SaMNP aqueous dispersion. After 5 days, the discs and surrounding CAMs were harvested and fixed for histological analysis. The remaining eggs were divided into 3 batches and on the 9th day, each egg was implanted with a xenograft of melanoma tissue (0.1 mL). This tissue was harvested by fine needle aspiration from the three C57BL/6 mice under sterile conditions. After the xenograft implantation, the CAMs were examined daily with an operator microscope equipped with lateral illumination and a digital camera system. Two days after the implantation of the melanoma xenografts, 3 CAMs randomly selected from each group were intravenously injected with a 0.25 mL dose of the SaMNP aqueous dispersion with an iron concentration of 0.356 mg/mL. This dose did not induce hemodynamic effects or changes in the normal evolution of the chicken embryo [38]. All eggs were incubated until day 15, when the melanoma xenografts were then harvested with the surrounding CAMs and were fixed within 48 h in 10% neutral buffered formalin.

2.5. Histological Analyses

Formalin fixed melanoma xenografts and antibiogram discs with surrounded CAM samples were processed using standard histological methods for paraffin embedding. Tissue sections in 5 μ m thicknesses were stained by conventional (hematoxylin and eosin, and azan trichrome) or specific (Perl's Prussian blue for Fe³⁺ ion evidence) techniques and were examined under light microscopy for morphological and semi-quantitative morphometric evaluation. To determine the vascular density, we divided each harvested disc into a randomly chosen diameter (with a length of 6 mm) and all the vessels present on the CAM below the test discs were counted under 20 \times microscope magnification. The thickness of the CAM was measured at the edges of each test disc. For control values, we randomly selected sections 6 mm long through the CAM located outside the tested area. We counted the vessels and measured the thickness of the CAM at the extremities of each selected area. The data obtained were statistically processed using SPSS software. The number of vessels per the disc diameter and CAM thickness were averaged for each experimental setup and were compared using a one-way ANOVA with Tukey's post hoc analysis. In all cases, $P < 0.05$ was used to indicate a statistical significance.

3. Results

3.1. Morphological Effects of SaMNPs on the CAM Assay

Changes in the morphology of the CAM that surrounded the test discs were observed under a stereomicroscope three days after implantation. A pro-angiogenic effect (an increase in the number of CAM vessels and wheel-spoke patterns of the vessels converging toward the implanted disc) was recorded in the CAM surrounding the saline-impregnated discs. In contrast, an anti-angiogenic effect (lack of new blood vessel formation) on the CAM vessels around the SaMNP-impregnated discs was observed (Figure 1a–c).

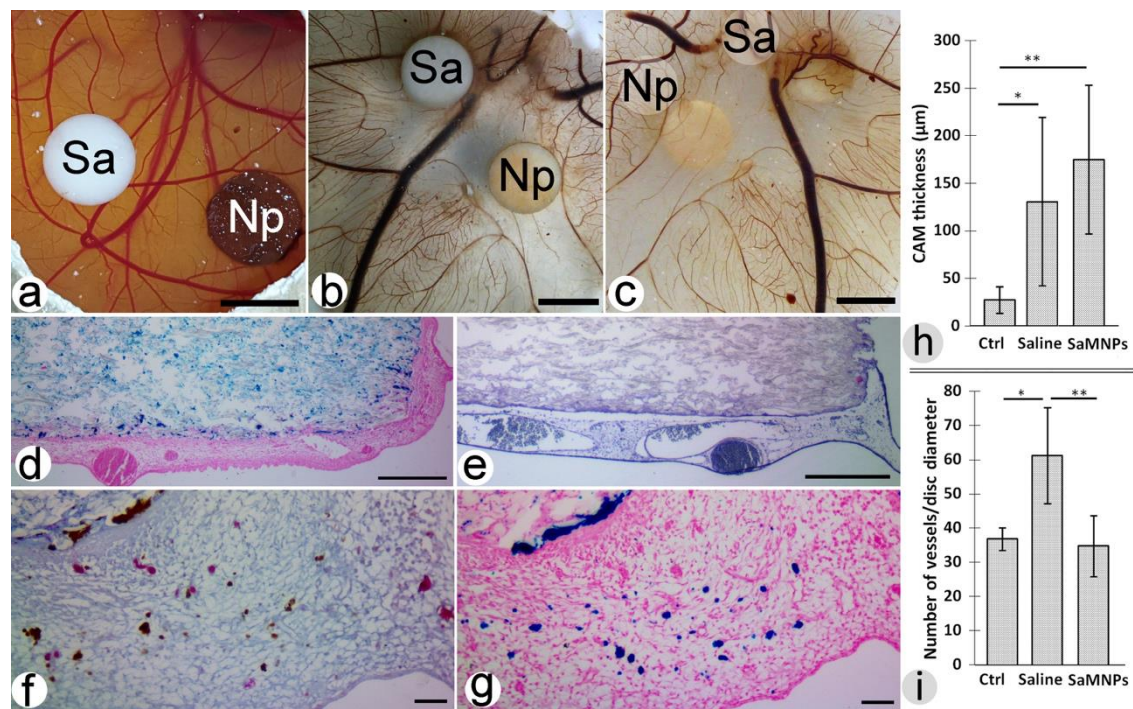


Figure 1. The morphological effects of SaMNPs on the CAM assay. (a) Discs where implantation occurred were pre-soaked with saline (Sa) and SaMNPs (Np) on a seven-day-old CAM; (b,c) Formalin fixed discs with surrounding a CAM (top and bottom view); (d,f,g) Histological sections through the Np-disc; (e) histological section through the Sa-disc; thickness (h) and counted vessels (i) variations on the normal CAM (Ctrl), Np-disc, and Sa-disc underneath the CAM (* $p < 0.05$; ** $p < 0.001$). Hematoxylin & eosin (e), Perl's Prussian blue (d,g) and Trichrome azan (f) staining; Bar = 5 mm (a–c); 100 µm (d,e); 10 µm (f,g).

Unlike the normal membrane that had a thickness of 27.3 ± 13.8 µm and 36.8 ± 3.3 vessels with a length of 6 mm, we found a thickness of 130.7 ± 88.3 µm and 61.27 ± 14.1 vessels/6 mm in the CAM below saline-impregnated discs 174.7 ± 78.2 µm and 34.7 ± 8.9 in the CAM below SaMNP-impregnated discs, respectively. We observed a significant global difference in the CAM thickness $F(2,21) = 9.741$, $p < 0.001$, and post hoc comparisons indicated a relevant difference between control and saline values ($p = 0.017$), and between control and SaMNP values ($p < 0.001$) (Figure 1h). We found a significant global difference between the number of vessels per disc diameter, $F(2,30) = 24.909$, $p < 0.001$; the post hoc comparisons indicated an important difference between saline and control values, and saline and SaMNP values ($p < 0.001$) (Figure 1i).

In addition, saline-impregnated discs induced the thickening of the underlying CAM mainly by increasing the number and diameter of the vessels, as opposed to SaMNP-impregnated discs that determined an increase in the density of collagen fibers, among which nanoparticle deposits were identified (Figure 1d–g).

3.2. Macroscopic Assessments of B16F10 Xenografts

The volume of murine melanoma xenografts began to increase from the second day following the implantation on the CAM. No angiogenesis was observed in the CAM around the implanted xenograft.

3.2.1. Untreated Xenografts

The continuous increase in xenograft volume, the formation of metastases both near and at a distance from the site of implantation, and occasionally the appearance of small hemorrhages in the thickness of the CAM around the implanted area were all main morphological features of the untreated melanoma xenografts (Figure 2d–f).

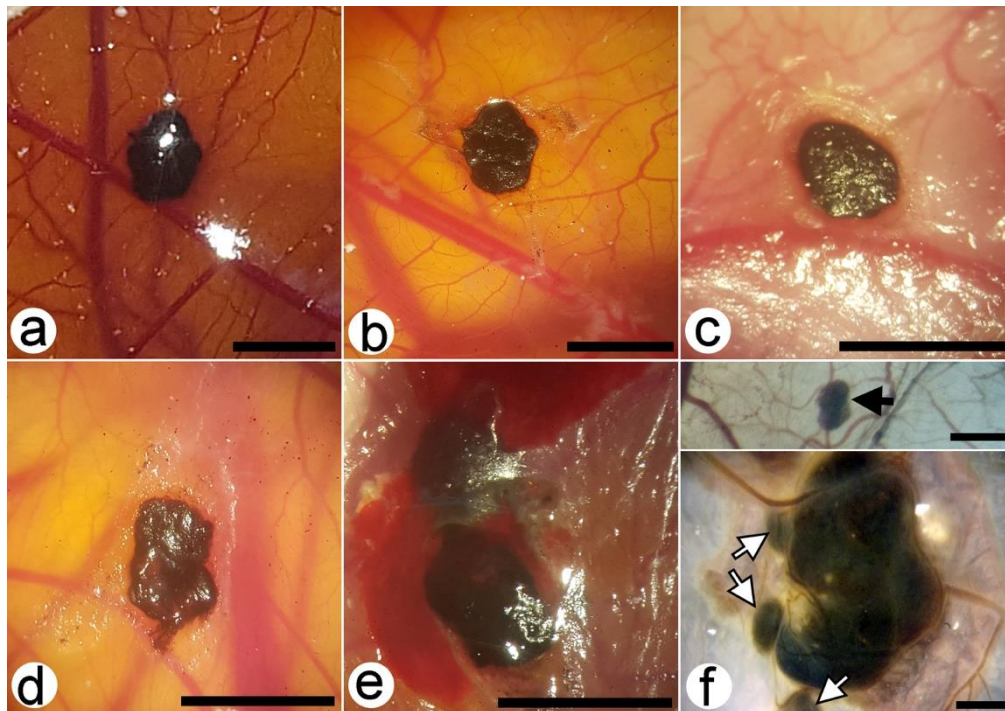


Figure 2. Macroscopic features of treated (a–c) and untreated (d–f) B16F10 xenografts implanted on nine-day-old CAM. Recent implanted (a), two-day-old (b,d), and five-day-old (c,e,f) B16F10 xenografts. Local ((f), white arrows) and distant ((f), black arrow) metastases arising from an untreated xenograft (formalin fixed CAM, bottom view). Bar = 5 mm (a–e); 1 mm (f).

3.2.2. SaMNP Treated Xenografts

The effects of slowing tumor growth and reducing the melanoma cells' ability to locally metastasize, along with its lack of distant metastases and bleeding in the CAM surrounding the implanted area were observed in murine xenografts treated by intravenous injections of SaMNP aqueous dispersions (Figure 2a–c).

3.3. Microscopic Assessments of B16F10 Xenografts

3.3.1. Untreated Xenografts

Heterogeneous melanoma cells with an epithelioid or spindle type and a high mitotic index and occasional areas of focal necrosis were morphological features observed in the untreated xenografts. Other features included the development of large intratumoral cavernous vascular spaces delimited by tumor cells that were filled with the chick's blood (nucleated erythrocytes). There were no structural changes in the CAM underlying the implant. Numerous vessels originating in the CAM's vessels entered the thickness of the xenograft to come into close contact with the lacunar system formed by the tumor cells. In some tumor areas, there was a rich hematic infiltrate between the tumor cells, which seemed to be an initial stage of the formation of intratumor blood canaliculi (Figure 3a–c). No direct connections between the CAM vessels and the intratumor blood canaliculi were identified in the studied sections.

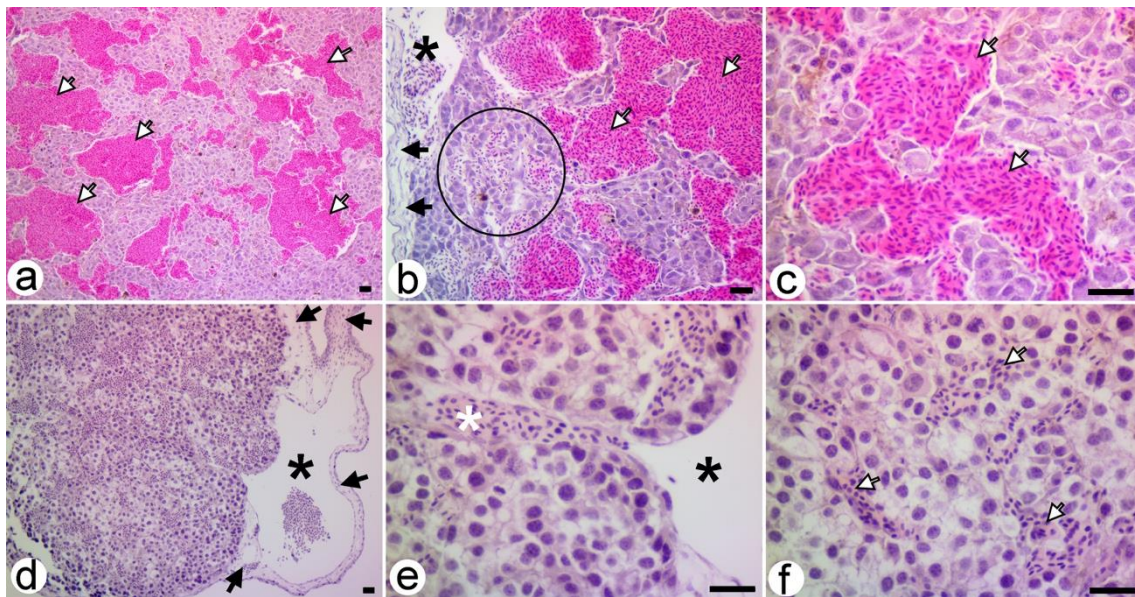


Figure 3. Histopathology of the five-day-old untreated B16F10 xenograft (a–c), and the local metastasis (d–f). Tumor areas with blood infiltrate (circle area) interposed between CAM vessels (black stars) and intratumoral cavernous vascular spaces filled with nucleated erythrocytes (white arrows). In the local metastases, a CAM vessel (white star) entering between the tumor cavernous vascular spaces can be observed. Black arrows show CAMs located underneath xenografts. Hematoxylin and Eosin staining. Bar = 25 μ m.

The processes of the tumor invasion by the CAM vessels and the formation of blood-filled vascular spaces delimited by the tumor cells were observed in the metastases around the implant (Figure 3d–f).

3.3.2. SaMNP-Treated Xenografts

Extensive tumor necrosis, atypical tumor cells, a lack of formation in intratumoral cavernous vascular spaces, chicken blood infiltrates, and vessels of CAM origin were the main morphological features that distinguished the treated xenografts from the untreated ones. Rare nests of melanoma cells, some with plasma membrane blebbing and pyknotic or fragmented nuclei, apoptotic bodies and extracellular exudates were observed scattered in the tumor necrosis mass and located mainly in the CAM vicinity (Figure 4a). Most of these tumor cells had intracytoplasmic deposits of SaMNPs with a perinuclear disposition highlighted by Perl's Prussian blue staining (Figure 4b).

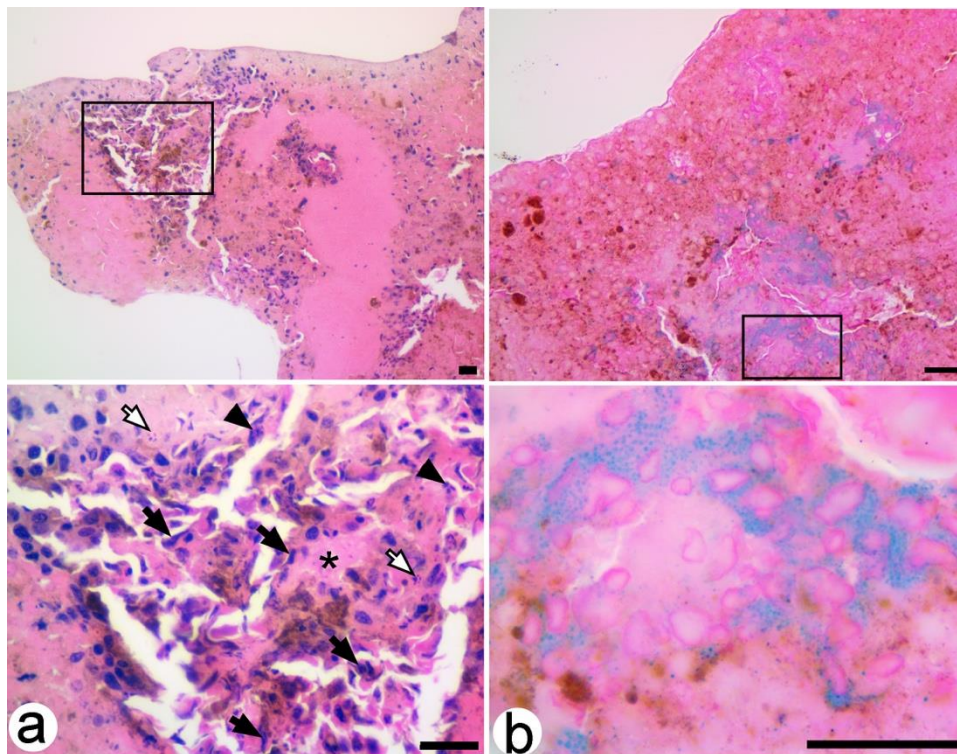


Figure 4. Histopathology of a B16F10 xenograft three days after SaMNP treatment. Area of tumor necrosis (a) with foci of melanoma cells presenting pyknotic (black arrows) or fragmented (black arrowheads) nuclei, apoptotic bodies (white arrows), and extracellular exudates (black star). Intracytoplasmic Perl's positive iron deposits with perinuclear disposition in the tumor necrosis area (b). Hematoxylin & eosin (a) and Perl's Prussian blue (b) staining. Bar = 25 μ m.

4. Discussion

The increase in the number of vessels can be considered an angiogenic effect induced by the saline pre-loaded discs, which represents an inflammatory response of the CAM to a foreign body [38,39]. The decrease in the number of vessels in the area of the SaMNP pre-soaked discs can be produced by the salicylate coating of the nanoparticles that has a well-known antiangiogenic effect produced by several mechanisms, such as the modulation of the circulating angiogenic proteins [40], the down-regulation of the glucose transporter 1 [41], the inhibition of the endothelial cells remodeling or apoptosis of microvascular endothelial cells [42], the perturbation of the EGFR axis [26], the inhibition of the COX isoforms [43], etc.

The quantitative modification of the collagen tissue observed in the case of SaMNP pre-soaked discs is due to the stimulation of the extracellular matrix production [44] and most likely the fibroblast's proliferative activities [45] exhibited by iron oxide nanoparticles.

The growth pattern of xenografts implanted on the membrane is similar to that described for other tumors [28,36,46]. Penetration of proliferating CAM vasculature into the B16F10 xenograft correlates with the beginning of its volume increase and marks the end of the avascular phase of xenograft growth [28]. In our study, this took about two days, thus determining the moment of intravenous administration of the SaMNP aqueous dispersion.

The slowing or stopping of the tumor growth observed in the B16F10 xenografts treated with an SaMNP aqueous dispersion can be attributed to the antiangiogenic effects of the salicylate coating of the nanoparticles. By blocking the entry of the CAM vessels inside the implanted xenograft, the salicylic acid became responsible for the appearance of the extended areas of intratumor necrosis and autolysis. Tumor regression in the treated xenografts was accompanied by apoptosis, which was present especially in the areas with melanoma cells loaded with SaMNP. Melanoma cell apoptosis can

be induced by multiple mechanisms manifested by each of the components of the SaMNP structure: the salicylic acid coating [17,23] and the iron oxide core respectively [47,48].

The enhanced permeability and retention effect [8,16] can explain the preferential accumulation of SaMNPs within B16F10 xenografts and their absence from normal CAM structures.

5. Conclusions

This study demonstrated the availability of the CAM model as a tool for testing the therapeutic properties of newly synthesized nanocomposites on melanoma xenotransplants.

The iron oxide nanoparticles functionalized with salicylic acid had a therapeutic potential in B16F10 melanoma due to the synergistic action of the two components of its structure: the coating of salicylic acid with anti-angiogenic and chemotherapeutic action and the core of iron oxides with cytotoxic action.

Author Contributions: Conceptualization, M.C.P., I.M., and S.A.B; Data curation, Ş.O.P.; Formal analysis, O.M.M.; Investigation, M.C.P., I.M., S.A.B, Ş.O.P., and O.M.M.; Methodology, I.M. and S.A.B; Project administration, I.M.; Resources, M.C.P., Ş.O.P., and D.E.M.; Writing—original draft, M.C.P., Ş.O.P., and O.M.M.; Writing—review & editing, I.M., S.A.B., and D.E.M. All authors have read and agreed to the published version of the manuscript.

Funding: This research received no external funding.

Acknowledgments: We wish to thank to Livia Sima from The Institute of Biology of the Romanian Academy for B16F10 melanoma cells donation.

Conflicts of Interest: The authors declare no conflict of interest.

References

- Schadendorf, D.; Fisher, D.E.; Garbe, C.; Gershenwald, J.E.; Grob, J.J.; Halpern, A.; Herlyn, M.; Marchetti, M.A.; McArthur, G.; Ribas, A.; et al. Melanoma. *Nat. Rev. Dis. Prim.* **2015**, *1*, 15003. [[CrossRef](#)] [[PubMed](#)]
- Domingues, B.; Lopes, J.M.; Soares, P.; Pópulo, H. Melanoma treatment in review. *Immunotargets Ther.* **2018**, *7*, 35–49. [[CrossRef](#)] [[PubMed](#)]
- Garbe, C.; Eigentler, T.K.; Keilholz, U.; Hauschild, A.; Kirkwood, J.M. Systematic Review of Medical Treatment in Melanoma: Current Status and Future Prospects. *Oncologist* **2011**, *16*, 5–24. [[CrossRef](#)] [[PubMed](#)]
- Lloyd-Hughes, H.; Shiatis, A.E.; Pabari, A.; Mosahebi, A.; Seifalian, A. Current and Future Nanotechnology Applications in the Management of Melanoma: A Review. *J. Nanomed. Nanotechnol.* **2015**, *6*, 6. [[CrossRef](#)]
- Bombelli, F.B.; Webster, C.A.; Moncrieff, M.; Sherwood, V. The scope of nanoparticle therapies for future metastatic melanoma treatment. *Lancet Oncol.* **2014**, *15*, e22–e32. [[CrossRef](#)]
- Hafeez, A.; Kazmi, I. Dacarbazine nanoparticle topical delivery system for the treatment of melanoma. *Sci. Rep.* **2017**, *7*, 16517. [[CrossRef](#)] [[PubMed](#)]
- Cruz, N.; Pinho, J.O.; Soveral, G.; Ascensão, L.; Matela, N.; Reis, C.; Gaspar, M.M. A Novel Hybrid Nanosystem Integrating Cytotoxic and Magnetic Properties as a Tool to Potentiate Melanoma Therapy. *Nanomaterials* **2020**, *10*, 693. [[CrossRef](#)]
- Janko, C.; Ratschker, T.; Nguyen, K.; Zschiesche, L.; Tietze, R.; Lyer, S.; Alexiou, C. Functionalized Superparamagnetic Iron Oxide Nanoparticles (SPIONs) as Platform for the Targeted Multimodal Tumor Therapy. *Front. Oncol.* **2019**, *9*, 59. [[CrossRef](#)]
- Tang, J.Q.; Hou, X.Y.; Yang, C.S.; Li, Y.X.; Xin, Y.; Guo, W.W.; Wei, Z.P.; Liu, Y.Q.; Jiang, G. Recent developments in nanomedicine for melanoma treatment. *Int. J. Cancer* **2017**, *141*, 646–653. [[CrossRef](#)]
- Park, S. Nano-mechanical phenotype as a promising biomarker to evaluate cancer development, progression, and anti-cancer drug efficacy. *J. Cancer Prev.* **2016**, *21*, 73–80. [[CrossRef](#)]
- Slominski, R.M.; Zmijewski, M.A.; Slominski, A.T. The role of melanin pigment in melanoma. *Exp. Dermatol.* **2015**, *24*, 258–259. [[CrossRef](#)] [[PubMed](#)]
- Sarna, M.; Zadlo, A.; Czuba-Pelech, B.; Urbanska, K. Nanomechanical Phenotype of Melanoma Cells Depends Solely on the Amount of Endogenous Pigment in the Cells. *Int. J. Mol. Sci.* **2018**, *19*, 607. [[CrossRef](#)] [[PubMed](#)]
- Sarna, M.; Krzykawska-Serda, M.; Jakubowska, M.; Zadlo, A.; Urbanska, K. Melanin presence inhibits melanoma cell spread in mice in a unique mechanical fashion. *Sci. Rep.* **2019**, *9*, 9280. [[CrossRef](#)] [[PubMed](#)]

14. Palanisamy, S.; Wang, Y.M. Superparamagnetic iron oxide nanoparticulate system: Synthesis, targeting, drug delivery and therapy in cancer. *Dalton Trans.* **2019**, *48*, 9490–9515. [CrossRef] [PubMed]
15. Kim, T.H.; Lee, S.; Chen, X. Nanotheranostics for personalized medicine. *Expert Rev. Mol. Diagn.* **2013**, *13*, 257–269. [CrossRef]
16. Rybka, J.D. Radiosensitizing properties of magnetic hyperthermia mediated by superparamagnetic iron oxide nanoparticles (SPIONs) on human cutaneous melanoma cell lines. *Rep. Pract. Oncol. Radiother.* **2019**, *24*, 152–157. [CrossRef]
17. Shiff, S.J.; Shivaprasad, P.; Santini, D.L. Cyclooxygenase inhibitors: Drugs for cancer prevention. *Curr. Opin. Pharmacol.* **2003**, *3*, 352–361. [CrossRef]
18. Sawaoka, H.; Tsuji, S.; Tsujii, M.; Gunawan, E.S.; Sasaki, Y.; Kawano, S.; Hori, M. Cyclooxygenase inhibitors suppress angiogenesis and reduce tumor growth in vivo. *Lab. Invest.* **1999**, *79*, 1469–1477. Available online: <https://pubmed.ncbi.nlm.nih.gov/10616198/> (accessed on 9 April 2020).
19. Thun, M.J.; Henley, S.J.; Patrono, C. Nonsteroidal anti-inflammatory drugs as anticancer agents: Mechanistic, pharmacologic, and clinical issues. *J. Natl. Cancer Inst.* **2002**, *94*, 252–266. [CrossRef]
20. Chan, A.T.; Ogino, S.; Fuchs, C.S. Aspirin and the risk of colorectal cancer in relation to the expression of COX-2. *N. Engl. J. Med.* **2007**, *356*, 2131–2142. [CrossRef]
21. Xu, X.M.; Sansores-Garcia, L.; Chen, X.M.; Matijevic-Aleksic, N.; Du, M.; Wu, K.K. Suppression of inducible cyclooxygenase 2 gene transcription by aspirin and sodium salicylate. *Proc. Natl. Acad. Sci. USA* **1999**, *96*, 5292–5297. [CrossRef]
22. Yin, M.J.; Yamamoto, Y.; Gaynor, R.B. The anti-inflammatory agents aspirin and salicylate inhibit the activity of I κ B kinase- β . *Nature* **1998**, *396*, 77–80. [CrossRef] [PubMed]
23. Zimmermann, K.C.; Waterhouse, N.J.; Goldstein, J.C.; Schuler, M.; Green, D.R. Aspirin induces apoptosis through release of cytochrome c from mitochondria. *Neoplasia* **2000**, *2*, 505–513. [CrossRef]
24. Nunez, L.; Valero, R.A.; Senovilla, L.; Sanz-Blasco, S.; García-Sancho, J.; Villalobos, C. Cell proliferation depends on mitochondrial Ca²⁺ uptake: Inhibition by salicylate. *J. Physiol.* **2006**, *571* (Pt 1), 57–73. [CrossRef]
25. Spitz, G.A.; Furtado, C.M.; Sola-Penna, M.; Zancan, P. Acetylsalicylic acid and salicylic acid decrease tumor cell viability and glucose metabolism modulating 6-phosphofructo-1-kinase structure and activity. *Biochem. Pharmacol.* **2009**, *77*, 46–53. [CrossRef] [PubMed]
26. Bashir, A.I.J.; Kankipati, C.S.; Jones, S.; Newman, R.M.; Safrany, S.T.; Perry, C.J.; Nicholl, I.D. A novel mechanism for the anticancer activity of aspirin and salicylates. *Int. J. Oncol.* **2019**, *54*, 1256–1270. [CrossRef] [PubMed]
27. Deryugina, I.E.; Quigley, P.J. Chick embryo chorioallantoic membrane model systems to study and visualize human tumor cell metastasis. *Histochem. Cell Biol.* **2008**, *130*, 1119–1130. [CrossRef] [PubMed]
28. Ribatti, D. The chick embryo chorioallantoic membrane in the study of tumor angiogenesis. *Rom. J. Morphol. Embryol.* **2008**, *49*, 131–135. Available online: <http://www.rjme.ro/RJME/resources/files/490208131135.pdf> (accessed on 9 April 2020). [PubMed]
29. Nowak-Sliwinska, P.; Segura, T.; Iruela-Arispe, M.L. The chicken chorioallantoic membrane model in biology, medicine and bioengineering. *Angiogenesis* **2014**, *17*, 779–804. [CrossRef]
30. Naik, M.; Brahma, P.; Dixit, M.A. Cost-Effective and Efficient Chick Ex-Ovo CAM Assay Protocol to Assess Angiogenesis. *Methods Protoc.* **2018**, *1*, 19. [CrossRef]
31. Vargas, A.; Zeisser-Labouèbe, M.; Lange, N.; Gurny, R.; Delie, F. The chick embryo and its chorioallantoic membrane (CAM) for the in vivo evaluation of drug delivery systems. *Adv. Drug Deliv. Rev.* **2007**, *59*, 1162–1176. [CrossRef]
32. DeBord, L.C.; Pathak, R.R.; Villaneuva, M.; Liu, H.C.; Harrington, D.A.; Yu, W.; Lewis, M.T.; Sikora, A.G. The chick chorioallantoic membrane (CAM) as a versatile patient-derived xenograft (PDX) platform for precision medicine and preclinical research. *Am. J. Cancer Res.* **2018**, *8*, 1642–1660. Available online: <https://www.ncbi.nlm.nih.gov/pmc/articles/PMC6129484/pdf/ajcr0008-1642.pdf> (accessed on 9 April 2020). [PubMed]
33. Kalirai, H.; Shahidipour, H.; Coupland, S.E.; Luyten, G. Use of the Chick Embryo Model in Uveal Melanoma. *Ocul. Oncol. Pathol.* **2015**, *1*, 133–140. [CrossRef]
34. Buteică, S.A.; Mihaiescu, D.E.; Rogoveanu, I.; Mărgăritescu, D.N.; Mîndrilă, I. Chick Chorioallantoic Membrane Model as a Preclinical Tool for Nanoparticles Biology Study. *Rom. Biotechnol. Lett.* **2016**, *21*, 11684–11690. Available online: <https://e-repository.org/rbl/vol.21/iss.4/9.pdf> (accessed on 9 April 2020).

35. Vu, B.T.; Shahin, S.A.; Croissant, J.; Fatieiev, Y.; Matsumoto, K.; Le-Hoang Doan, T.; Yik, T.; Simargi, S.; Conteras, A.; Ratliff, L.; et al. Chick chorioallantoic membrane assay as an in vivo model to study the effect of nanoparticle-based anticancer drugs in ovarian cancer. *Sci. Rep.* **2018**, *8*, 8524. [CrossRef]
36. Mîndrilă, I.; Buteică, S.A.; Mihaiescu, D.E.; Burada, F.; Mîndrilă, B.; Predoi, M.C.; Pirici, I.; Fudulu, A.; Croitoru, O. Magnetic nanoparticles-based therapy for malignant mesothelioma. *Rom. J. Morphol. Embryol.* **2017**, *58*, 457–463. Available online: <http://www.rjme.ro/RJME/resources/files/580217457463.pdf> (accessed on 9 April 2020).
37. Mîndrilă, I.; Buteică, S.A.; Mihaiescu, D.E.; Badea, G.; Fudulu, A.; Mărgăritescu, D.N. Fe₃O₄/salicylic acid nanoparticles versatility in magnetic mediated vascular nanoblockage. *J. Nanopart. Res.* **2016**, *18*, 10. [CrossRef]
38. Mihaiescu, D.E.; Buteică, A.S.; Neamțu, J.; Istrati, D.; Mîndrilă, I. Fe₃O₄/Salicylic acid nanoparticles behavior on chick CAM vasculature. *J. Nanopart. Res.* **2013**, *15*, 1857. [CrossRef]
39. Lemus, D.; Dabancens, A.; Illanes, J.; Fuenzalida, M.; Guerrero, A.; López, C. Antiangiogenic effect of betamethasone on the chick cam stimulated by TA3 tumor supernatant. *Biol. Res.* **2001**, *34*, 227–236. [CrossRef]
40. Holmes, C.E.; Jasielc, J.; Levis, J.E.; Skelly, J.; Muss, H.B. Initiation of aspirin therapy modulates angiogenic protein levels in women with breast cancer receiving tamoxifen therapy. *Clin. Transl. Sci.* **2013**, *6*, 386–390. [CrossRef]
41. Hu, Y.; Lou, X.; Wang, R.; Sun, C.; Liu, X.; Liu, S.; Wang, Z.; Ni, C. Aspirin, a Potential GLUT1 Inhibitor in a Vascular Endothelial Cell Line. *Open Med. (Wars)* **2019**, *14*, 552–560. [CrossRef] [PubMed]
42. Borthwick, G.M.; Sarah Johnson, A.; Partington, M.; Burn, J.; Wilson, R.; Arthur, H.M. Therapeutic levels of aspirin and salicylate directly inhibit a model of angiogenesis through a Cox- independent mechanism. *FASEB J.* **2006**, *20*, 2009–2016. [CrossRef] [PubMed]
43. Mojid Mondol, M.A. Antiangiogenic Study of Two Nonsteroidal Antiinflammatory Compounds Using Chick Chorioallantoic Membrane Assay. *J. Med. Sci.* **2006**, *6*, 609–614. [CrossRef]
44. Blyakhman, F.A.; Makarova, E.B.; Fadeyev, F.A.; Lugovets, D.V.; Safronov, A.P.; Shabadrov, P.A.; Shklyar, T.F.; Melnikov, G.Y.; Orue, I.; Kurlyandskaya, G.V. The Contribution of Magnetic Nanoparticles to Ferrogel Biophysical Properties. *Nanomaterials* **2019**, *9*, 232. [CrossRef] [PubMed]
45. Casco, M.; Olsen, T.; Herbst, A.; Evans, G.; Rothermel, T.; Pruett, L.; Simionescu, D.; Visconti, R.; Alexis, F. Iron Oxide Nanoparticles Stimulates Extra-Cellular Matrix Production in Cellular Spheroids. *Bioengineering* **2017**, *4*, 4. [CrossRef]
46. Buteică, S.A.; Mîndrilă, I.; Mihaiescu, D.E.; Purcaru, S.O.; Dricu, A.; Nicolicescu, C.; Neamțu, J. In vitro and in vivo effects of Fe₃O₄/salicylic acid magnetic nanoparticles on the human glioblastoma cells. *Dig. J. Nanomater. Biostruct.* **2014**, *9*, 959–965. Available online: http://www.chalcogen.ro/959_Buteica.pdf (accessed on 9 April 2020).
47. Feng, Q.; Liu, Y.; Huang, J.; Chen, K.; Huang, J.; Xiao, K. Uptake, distribution, clearance, and toxicity of iron oxide nanoparticles with different sizes and coatings. *Sci. Rep.* **2018**, *8*, 2082. [CrossRef]
48. He, C.; Jiang, S.; Jin, H.; Chen, S.; Lin, G.; Yao, H.; Wang, X.; Mi, P.; Ji, Z.; Lin, Y.; et al. Mitochondrial electron transport chain identified as a novel molecular target of SPIO nanoparticles mediated cancer-specific cytotoxicity. *Biomaterials* **2016**, *83*, 102–114. [CrossRef]

